

Optimization of the passive components of the Modular Multilevel Matrix Converter for Drive Applications

Felix Kammerer, Johannes Kolb, Michael Braun
 Elektrotechnisches Institut (ETI) - Electrical Drives and Power Electronics
 Karlsruhe Institute of Technology (KIT), Kaiserstr. 12, 76131 Karlsruhe, Germany
 Tel.: +49 721 608 42461, E-mail: felix.kammerer@kit.edu

Abstract

The Modular Multilevel Matrix Converter (M3C) is a new topology which extends the Modular Multilevel Converter (M2C) family for converters to low speed drive applications. The energy pulsation and therefore the amount of the installed capacitance is very important for the design of such a converter. This paper presents a method to estimate the required amount of capacitance for a given application. Additionally, the design of a newly proposed coupled z-winding arm inductor is explained. It is verified that the use of this inductor allows considerable savings of core and coil material.

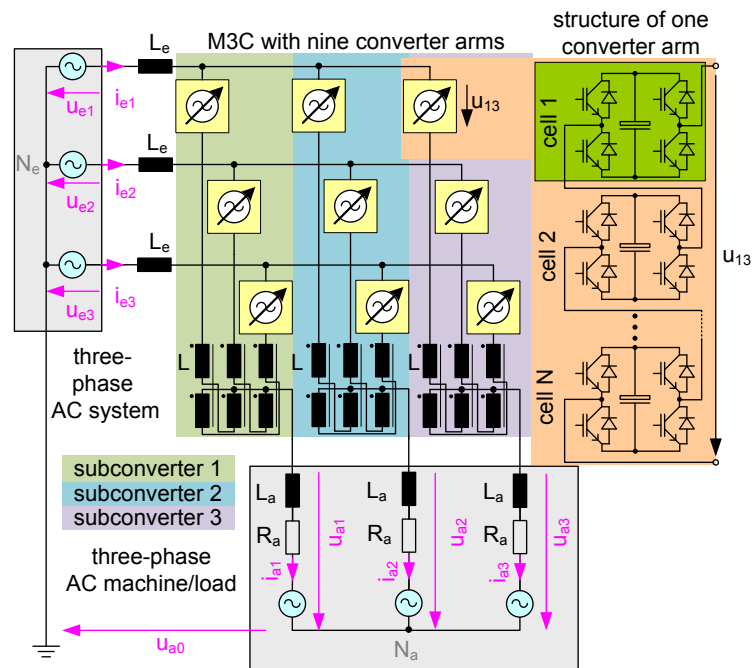


Figure 1: Modular Multilevel Matrix Converter (M3C) with coupled three-phase z-winding arm inductors L

1 Introduction

The Modular Multilevel Matrix Converter shown in fig. 1 has been presented in 2001 without the arm inductors L [1]. [2] and [3] present control principles based on the space vector modulation which are difficult to implement in a M3C with more than one cell per arm. In [4] conventional arm inductors are added and a feedforward control is implemented, which is extended in [5] with a DC-circulating current balancing control. The system works in steady state, but the dynamic

behaviour is not clear. [6] presents design principles and the control of the M3C for high power low speed drives. The control principles are based on the power balance and include a method to reduce the installed amount of capacitance. In [7] a cascaded feedback control system with inner arm current controllers and superimposed capacitor voltage controllers is presented. The operation at steady state is shown, but the dynamic behavior is not clear. In [8] the coupled z-winding arm inductors (fig. 1) are presented together with a cascaded vector control scheme. This control scheme allows the independent input and output current control and the complete equalization of the energy stored in the converter arms with an average, horizontal and vertical balancing control. The stable operation is verified even under dynamic changes of the operation point.

1.1 Voltages and currents in one subconverter

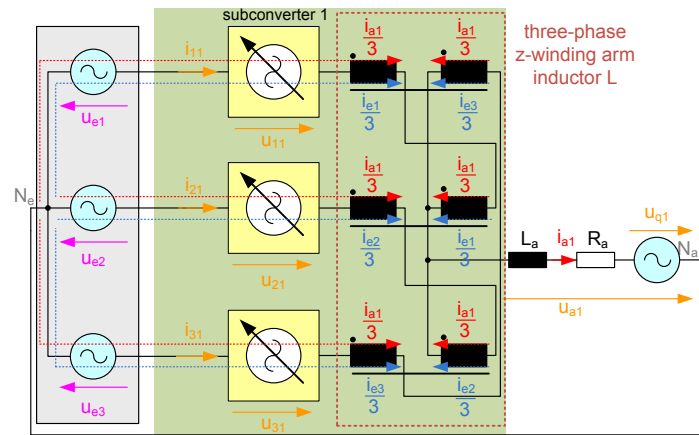


Figure 2: Subconverter with coupled three-phase z-winding arm inductors L

The M3C (see fig. 1) analyzed in this paper consists of 3 identical subconverters with 3 converter arms and a coupled z-winding arm inductor L (fig. 2). Each converter arm connects one input phase via the three-phase z-winding arm inductor L with one output phase. It consists of N series-connected cells which are built as an H-bridge with a DC-capacitor. The detailed relations of currents and voltages inside of a subconverter are derived in [8] and given here for steady state operation. The arm currents i_{11}, i_{21}, i_{31} contain the following components:

$$\begin{aligned}
 i_{11} &= \frac{i_{e1}}{3} + \frac{i_{a1}}{3} = \frac{\hat{I}_e}{3} \cdot \cos(\omega_e t + \varphi_e) + \frac{\hat{I}_a}{3} \cdot \cos(\omega_a t + \gamma + \varphi_a) \\
 i_{21} &= \frac{i_{e2}}{3} + \frac{i_{a1}}{3} = \frac{\hat{I}_e}{3} \cdot \cos(\omega_e t - \frac{2\pi}{3} + \varphi_e) + \frac{\hat{I}_a}{3} \cdot \cos(\omega_a t + \gamma + \varphi_a) \\
 i_{31} &= \frac{i_{e3}}{3} + \frac{i_{a1}}{3} = \frac{\hat{I}_e}{3} \cdot \cos(\omega_e t - \frac{4\pi}{3} + \varphi_e) + \frac{\hat{I}_a}{3} \cdot \cos(\omega_a t + \gamma + \varphi_a)
 \end{aligned} \tag{1}$$

φ_e and φ_a are the phase angles of the currents to the related voltages and γ is the initial phase angle between the input and output voltage system. Note that the arm currents can contain also internal currents i_i which are used for the energy balancing and energy pulsation reduction. The arm voltages which are generated by the converter arms without the consideration of the

Table 1: power components in converter arm 11

Component	power components
$+\frac{1}{6}\hat{U}_e \cdot \hat{I}_e \cdot \cos(\varphi_e)$	active input power
$+\frac{1}{6}\hat{U}_e \cdot \hat{I}_e \cdot \cos(2\omega_e t + \varphi_e)$	reactive power with $2f_e$
$-\frac{1}{6}\hat{U}_a \cdot \hat{I}_a \cdot \cos(\varphi_a)$	active output power
$-\frac{1}{6}\hat{U}_a \cdot \hat{I}_a \cdot \cos(2\omega_a t + 2\gamma + \varphi_a)$	reactive power with $2f_a$
$+\frac{1}{6}\hat{U}_e \cdot \hat{I}_a [\cos((\omega_e - \omega_a)t - \gamma - \varphi_a) - \cos((\omega_e - \omega_a)t - \gamma + \varphi_e)]$	reactive power with $f_e - f_a$
$+\frac{1}{6}\hat{U}_a \cdot \hat{I}_e [\cos((\omega_e + \omega_a)t + \gamma + \varphi_a) - \cos((\omega_e + \omega_a)t + \gamma + \varphi_e)]$	reactive power with $f_e + f_a$

inductor voltages are defined as:

$$\begin{aligned}
 u_{11} &= u_{e1} - u_{a1} = \hat{U}_e \cdot \cos(\omega_e t) - \hat{U}_a \cdot \cos(\omega_a t + \gamma) \\
 u_{21} &= u_{e2} - u_{a1} = \hat{U}_e \cdot \cos(\omega_e t - \frac{2\pi}{3}) - \hat{U}_a \cdot \cos(\omega_a t + \gamma) \\
 u_{31} &= u_{e3} - u_{a1} = \hat{U}_e \cdot \cos(\omega_e t - \frac{4\pi}{3}) - \hat{U}_a \cdot \cos(\omega_a t + \gamma)
 \end{aligned} \tag{2}$$

Using (1) and (2) the instantaneous arm power can be calculated:

$$p_{11} = u_{11} \cdot i_{11} \qquad p_{21} = u_{21} \cdot i_{21} \qquad p_{31} = u_{31} \cdot i_{31} \tag{3}$$

Table 1 shows the different power components of the converter arm 11. The other converter arms have similar power components, only the phase angles of the reactive power components are different. The active power components must sum up to zero to maintain the DC-capacitors of the converter arms at a given reference voltage. The input current amplitude \hat{I}_e can be calculated depending on the desired M3C output voltage \hat{U}_a and current amplitude \hat{I}_a (which also defines the M3C output power $P_a = \frac{3}{2} \cdot \hat{U}_a \cdot \hat{I}_a \cdot \cos(\varphi_a)$) and using $k = \frac{\hat{U}_a}{\hat{U}_e}$ which is the voltage relation between the input and output voltage amplitude:

$$0 = \frac{1}{6}\hat{U}_e \cdot \hat{I}_e \cdot \cos(\varphi_e) - \frac{1}{6}\hat{U}_a \cdot \hat{I}_a \cdot \cos(\varphi_a) \qquad \Rightarrow \hat{I}_e = k \cdot \hat{I}_a \cdot \frac{\cos(\varphi_a)}{\cos(\varphi_e)} \tag{4}$$

2 Estimation of the energy pulsation in the converter arms

The energy pulsation \tilde{p}_{11} of one converter arm 11 which has to be buffered by the arm capacitance can be calculated using the reactive power terms from table 1:

$$\begin{aligned}
 \tilde{p}_{11} &= \frac{P_a}{9} \left[+\frac{1}{\cos(\varphi_e)} \cos(2\omega_e t + \varphi_e) - \frac{1}{\cos(\varphi_a)} \cdot \cos(2v\omega_e t + 2\gamma + \varphi_a) \right. \\
 &\quad + \frac{1}{k} \cdot \frac{1}{\cos(\varphi_a)} \cdot \cos((1-v)\omega_e t - \gamma - \varphi_a) - \frac{k}{\cos(\varphi_e)} \cdot \cos((1-v)\omega_e t - \gamma + \varphi_e) \\
 &\quad \left. + \frac{1}{k} \cdot \frac{1}{\cos(\varphi_a)} \cdot \cos((1+v)\omega_e t + \gamma + \varphi_a) - \frac{k}{\cos(\varphi_e)} \cdot \cos((1+v)\omega_e t + \gamma + \varphi_e) \right] \tag{5}
 \end{aligned}$$

with the frequency transfer ratio $v = \frac{\omega_a}{\omega_e}$. The upper limit is calculated in order to estimate the maximum energy pulsation ΔW_{max} . Due to this, it is secured that the real energy variation can

not extend the calculated limit in steady state operation. ΔW_{max} is calculated by the sum of the integration of all different frequency terms from (5) over half a period:

$$\Delta W_{max} = \frac{P_a}{9 \cdot \omega_e} \left[\frac{1}{\cos(\varphi_e)} + \frac{1}{|v \cos(\varphi_a)|} + \left(\left| \frac{1}{k} \cdot \frac{1}{\cos(\varphi_a)} \right| + \left| \frac{k}{\cos(\varphi_e)} \right| \right) \cdot \left(\frac{2}{|1-v|} + \frac{2}{|1+v|} \right) \right] \quad (6)$$

Together with the allowed maximum voltage variation $\Delta u_{c,max}$ the required arm capacitance C_{arm} will be calculated to ([6]):

$$C_{arm} = k_s \cdot \frac{\Delta W_{max}}{U_{c,avg} \cdot \Delta u_{c,max}} \quad (7)$$

with the average arm capacitor voltage $U_{c,avg}$ and an additional safety factor $k_s = 2 \dots 3$ which may be used to get the time for the balancing of the energy stored in the M3C.

3 Advantages of the coupled z-winding arm inductor

In this section the amount of material needed for the core and the coils of the three-phase inductor is calculated for the series connection and the z-winding. Fig. 3 shows the physical layout of a three-phase inductor with 2 windings per inductor leg.

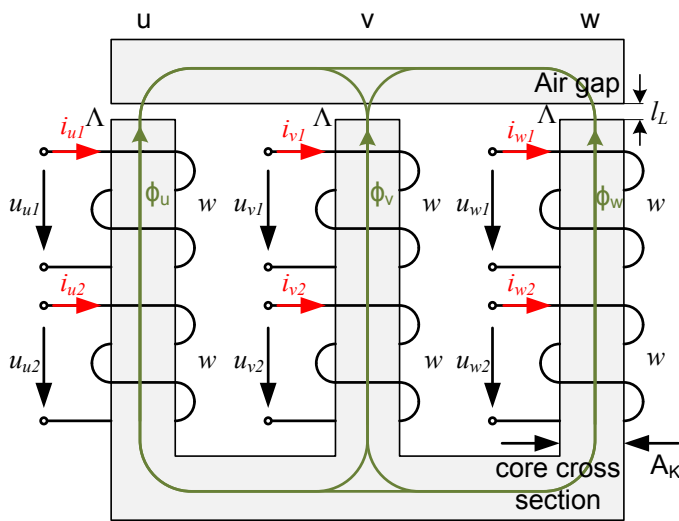


Figure 3: Physical layout of a three-phase inductor with 2 windings per inductor leg

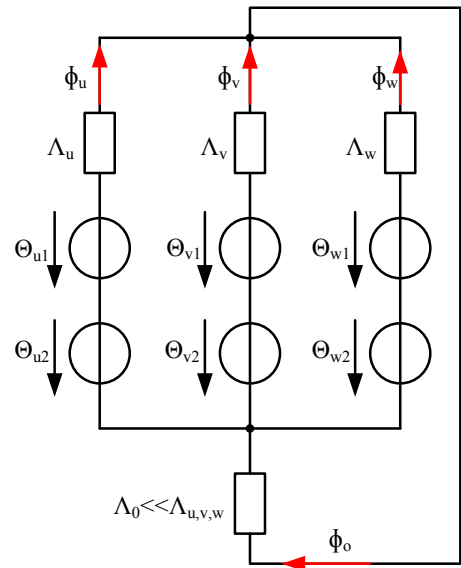


Figure 4: Equivalent magnetic circuit of the three-phase inductor

3.1 General considerations

Fig. 4 shows the equivalent magnetic circuit of the inductor. The current linkages $\Theta = w \cdot i$ are drawn as voltage sources which generate a corresponding magnetic flux Φ depending of the magnetic conductance Λ . Λ depends on the core cross section A_K and the equivalent air gap l_E , which considers also the length on the magnetic flux line in the core material l_{Fe} :

$$\Lambda = \mu_0 \cdot \frac{A_K}{l_L + \frac{l_{Fe}}{\mu_r Fe}} = \mu_0 \cdot \frac{A_K}{l_E} \quad (8)$$

We obtain the magnetic flux Φ inside of the three inductor core legs depending on the six current linkages by solving the equations from fig. 4:

$$\begin{aligned}\Phi_u &= +\frac{2}{3}\Lambda(\Theta_{u1} + \Theta_{u2}) - \frac{1}{3}\Lambda(\Theta_{v1} + \Theta_{v2}) - \frac{1}{3}\Lambda(\Theta_{w1} + \Theta_{w2}) \\ \Phi_v &= -\frac{1}{3}\Lambda(\Theta_{u1} + \Theta_{u2}) + \frac{2}{3}\Lambda(\Theta_{v1} + \Theta_{v2}) - \frac{1}{3}\Lambda(\Theta_{w1} + \Theta_{w2}) \\ \Phi_w &= -\frac{1}{3}\Lambda(\Theta_{u1} + \Theta_{u2}) - \frac{1}{3}\Lambda(\Theta_{v1} + \Theta_{v2}) + \frac{2}{3}\Lambda(\Theta_{w1} + \Theta_{w2})\end{aligned}\quad (9)$$

In case of

$$\Theta_{u1} + \Theta_{u2} + \Theta_{v1} + \Theta_{v2} + \Theta_{w1} + \Theta_{w2} \neq 0 \quad (10)$$

a common-mode flux Φ_0 is generated which can not flow inside of the inductor core:

$$\Phi_0 = \frac{3\Lambda \cdot \Lambda_0}{3\Lambda + \Lambda_0} \cdot \frac{1}{3} \cdot (\Theta_{u1} + \Theta_{u2} + \Theta_{v1} + \Theta_{v2} + \Theta_{w1} + \Theta_{w2}) = \frac{3\Lambda \cdot \Lambda_0}{3\Lambda + \Lambda_0} \cdot \Theta_0 \quad (11)$$

The self-inductance L_E is defined as relation between the magnetic flux linkage Ψ generated in the winding w and the current i following through it:

$$L_E = \frac{\Psi}{i} = \frac{w \cdot \Phi}{i} = \frac{w \cdot (\frac{2}{3}\Lambda \cdot \Theta)}{i} = \frac{w \cdot (\frac{2}{3}\Lambda \cdot w \cdot i)}{i} = w^2 \cdot \frac{2}{3}\Lambda \quad (12)$$

3.2 Series connection of two coils

For the series connection of two coils on one inductor leg the current linkage is defined as:

$$\begin{aligned}\Theta_u &= \Theta_{u1} + \Theta_{u2} = 2 \cdot w_R \cdot i_{u1} \\ \Theta_v &= \Theta_{v1} + \Theta_{v2} = 2 \cdot w_R \cdot i_{v1} \\ \Theta_w &= \Theta_{w1} + \Theta_{w2} = 2 \cdot w_R \cdot i_{w1}\end{aligned}\quad (13)$$

w_R is the number of turns per winding. The magnetic flux is calculated to:

$$\begin{aligned}\Phi_u &= \frac{2}{3}\Lambda w_R (+2i_{u1} - i_{v1} - i_{w1}) = 2\Lambda w_R i_{u1} \\ \Phi_v &= \frac{2}{3}\Lambda w_R (-i_{u1} + 2i_{v1} - i_{w1}) = 2\Lambda w_R i_{v1} \\ \Phi_w &= \frac{2}{3}\Lambda w_R (-i_{u1} - i_{v1} - 2i_{w1}) = 2\Lambda w_R i_{w1}\end{aligned}\quad (14)$$

with $i_{u1} + i_{v1} + i_{w1} = 0$ which is valid for the input currents i_e of the subconverter. The magnetic flux linkage is calculated using the number of turns $2w_R$:

$$\Psi_u = 4\Lambda w_R^2 i_{u1} \quad \Psi_v = 4\Lambda w_R^2 i_{v1} \quad \Psi_w = 4\Lambda w_R^2 i_{w1} \quad (15)$$

Finally, the inductance representing the series connection L_R is defined as:

$$L_R = \frac{\Psi_u}{i_{u1}} = \frac{\Psi_v}{i_{v1}} = \frac{\Psi_w}{i_{w1}} = 4\Lambda w_R^2 \quad (16)$$

The common-mode flux linkage Ψ_0 is generated depending on the magnetic conductance Λ_0 and the output current i_a :

$$\Psi_0 = 2 \cdot w_R \cdot \frac{3\Lambda \cdot \Lambda_0}{3\Lambda + \Lambda_0} \cdot \Theta_0 = 4 \cdot \frac{3\Lambda \cdot \Lambda_0}{3\Lambda + \Lambda_0} \cdot w_R^2 \cdot \frac{i_a}{3} \quad (17)$$

The inductance L_{R0} which is valid for the output current i_a is calculated to:

$$L_{R0} = \frac{\Psi_0}{i_a} = \frac{4}{3} \frac{3\Lambda \cdot \Lambda_0}{3\Lambda + \Lambda_0} w_R^2 < \frac{L_R}{3} \quad (18)$$

3.3 Connection as z-winding

The six windings can be connected as z-winding. The current linkage of the three inductor legs are defined as:

$$\begin{aligned}\Theta_u &= \Theta_{u1} + \Theta_{u2} = w_z \cdot (i_{u1} - i_{w1}) \\ \Theta_v &= \Theta_{v1} + \Theta_{v2} = w_z \cdot (i_{v1} - i_{u1}) \\ \Theta_w &= \Theta_{w1} + \Theta_{w2} = w_z \cdot (i_{w1} - i_{v1})\end{aligned}\quad (19)$$

w_z is the number of turns of one winding. The magnetic flux of the inductor legs is calculated to:

$$\begin{aligned}\Phi_u &= \Lambda w_z (i_{u1} - i_{w1}) \\ \Phi_v &= \Lambda w_z (i_{v1} - i_{u1}) \\ \Phi_w &= \Lambda w_z (i_{w1} - i_{v1})\end{aligned}\quad (20)$$

The magnetic flux linkage is given by:

$$\begin{aligned}\Psi_{uv} &= w_z \cdot (\Phi_u - \Phi_v) = w_z^2 \Lambda (i_{u1} - i_{w1} - i_{v1} + i_{u1}) = 3\Lambda w_z^2 i_{u1} \\ \Psi_{vw} &= w_z \cdot (\Phi_v - \Phi_w) = w_z^2 \Lambda (i_{v1} - i_{u1} - i_{w1} + i_{v1}) = 3\Lambda w_z^2 i_{v1} \\ \Psi_{wu} &= w_z \cdot (\Phi_w - \Phi_u) = w_z^2 \Lambda (i_{w1} - i_{v1} - i_{u1} + i_{w1}) = 3\Lambda w_z^2 i_{w1}\end{aligned}\quad (21)$$

with $i_{u1} + i_{v1} + i_{w1} = 0$ which is valid for the input currents i_e . The inductance for the input currents of the z-winding L_z is calculated to:

$$L_z = \frac{\Psi_{uv}}{i_{u1}} = \frac{\Psi_{vw}}{i_{v1}} = \frac{\Psi_{wu}}{i_{w1}} = 3\Lambda w_z^2 \quad (22)$$

The output current $i_a = i_{u1} + i_{v1} + i_{w1}$ does not generate any current linkage:

$$\Theta_0 = \frac{1}{3}(\Theta_u + \Theta_v + \Theta_w) = w_z \cdot \frac{1}{3}(i_{u1} - i_{w1} + i_{v1} - i_{u1} + i_{w1} - i_{v1}) = 0 \quad (23)$$

and therefore no magnetic flux. The inductance for the output currents i_a is

$$L_{z0} = 0 \quad (24)$$

3.4 Comparison of series connection and z-winding

To compare the inductance $L_z = L_R$ for the input currents i_e the number of turns w_z and w_R is compared:

$$L_z = L_R \quad 3\Lambda w_z^2 = 4\Lambda w_R^2 \quad \Rightarrow w_z = \frac{2}{\sqrt{3}} \cdot w_R \approx 1.155 \cdot w_R \quad (25)$$

The result is that about 15.5% more turns are needed to get the same inductance L_z as in the series connection L_R .

The currents flowing in the subconverter are defined in (1). For $k = 1$ the input and output currents have the same amplitude. In the z-winding only the input currents can generate a current linkage (see eq. (19)) and therefore a magnetic flux Φ which must be conducted in one leg of the inductor core with the cross section A_{Kz} :

$$\Phi_{uz} = \Lambda w_z \cdot (i_{u1} - i_{w1}) = \Lambda w_z \cdot \left(\frac{i_{e1}}{3} - \frac{i_{e3}}{3}\right) \Rightarrow \Phi_{z,max} = \Lambda w_z \cdot \frac{\sqrt{3}}{3} \cdot \hat{I}_e \quad (26)$$

In contrast using the series connection the input and output currents generate a current linkage (see eq. (13)) and therefore a magnetic flux Φ :

$$\Phi_{uR} = 2\Lambda \cdot w_R \cdot i_{u1} = 2\Lambda \cdot w_R \cdot \left(\frac{i_{e1}}{3} + \frac{i_{a1}}{3} \right) \Rightarrow \Phi_{R,max} = 2\Lambda \cdot w_R \cdot \frac{2}{3} \cdot \hat{I}_e \quad (27)$$

The ratio between (26) and (27) leads to:

$$2 = \frac{\Phi_{R,max}}{\Phi_{z,max}} \quad (28)$$

Using the same constant magnetic flux density $B = \frac{\Phi}{A_K} = const$ inside of the inductor core the z-winding needs a core with the half cross section:

$$A_{Kz} = \frac{A_{KR}}{2} \quad (29)$$

To sum it up, for the z-winding about 15.5% more turns to get the same inductance L_z as in the series connection L_R are needed, but the core cross section A_z and therefore the edge length of the inductor core is smaller by the factor $\sqrt{2}$. This leads to smaller diameters of the windings. In total, only about $\frac{2}{\sqrt{3}\sqrt{2}} \approx 81\%$ of the winding material is needed compared to the series connection using a similar current density. Altogether only half of the core material and about 81% of the winding material is needed compared to a conventional 3 phase inductor or conventional arm inductors presented in [4]. Additionally there is no influence of the z-winding inductor to the output current control which limits the dynamic control performance.

4 Simulation results

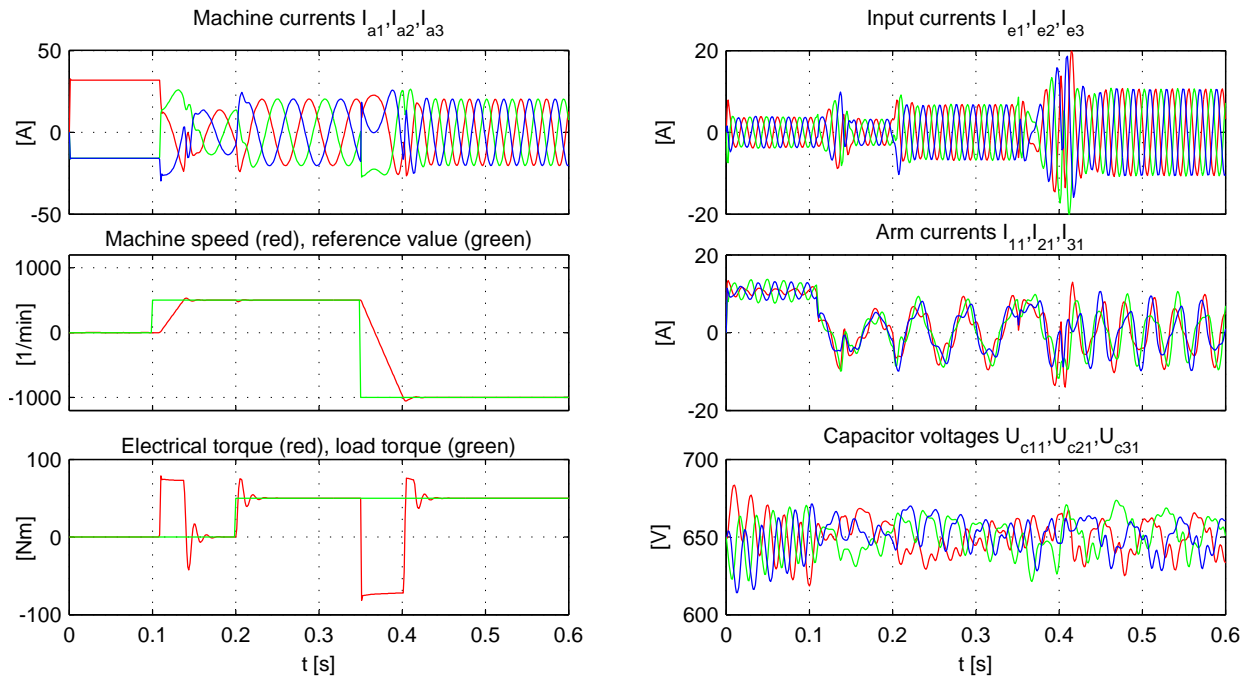


Figure 5: M3C with induction machine

Fig. 5 shows the M3C working together with an induction machine which is planned to use for the future laboratory prototype. At $t = 0$ s flux generating currents are feed in and at $t = 0.1$ s the

speed reference value is set to $n = 500\text{min}^{-1}$. At $t = 0.2\text{s}$ a load torque step with $M_L = 50\text{Nm}$ is applied. At $t = 0.35\text{s}$ the speed reference value is set zu $n = -1000\text{min}^{-1}$, therefor the direction of the power flow changes. The control system described in [8] is used and retains the system stable unter all circumstances.

5 Conclusion

This paper presents a method to estimate the maximum energy pulsation in the converter arms of the M3C. Additionally, a new three phase z-winding arm inductor L is explained for the M3C which allows considerable saving of core and coil materials. With this results it is possible to build a efficient M3C for high power low speed drive applications. Simulation results are used to verify the stable function and the presented design considerations of the passive components.

Acknowledgment

The authors would like to thank the DFG (German Research Foundation) which supports this research project.

References

- [1] R.W. Erickson and O.A. Al-Naseem. A new family of matrix converters. In *Industrial Electronics Society, 2001. IECON '01. The 27th Annual Conference of the IEEE*, volume 2, pages 1515 –1520 vol.2, 2001.
- [2] S. Angkititrakul and R.W. Erickson. Capacitor voltage balancing control for a modular matrix converter. In *Applied Power Electronics Conference and Exposition, 2006. APEC '06. Twenty-First Annual IEEE*, page 7 pp., march 2006.
- [3] S. Angkititrakul and R.W. Erickson. Control and implementation of a new modular matrix converter. In *Applied Power Electronics Conference and Exposition, 2004. APEC '04. Nineteenth Annual IEEE*, volume 2, pages 813 – 819 vol.2, 2004.
- [4] C. Oates. A methodology for developing chainlink converters. In *Power Electronics and Applications, 2009. EPE '09. 13th European Conference on*, pages 1 –10, sept. 2009.
- [5] C. Oates and G. Mondal. Dc circulating current for capacitor voltage balancing in modular multilevel matrix converter. *EPE 2011 Birmingham*, aug. 2011.
- [6] A.J. Korn, M. Winkelkemper, P. Steimer, and J.W. Kolar. Direct modular multi-level converter for gearless low-speed drives. *EPE 2011 Birmingham*, aug. 2011.
- [7] D. C. Ludois, J. K. Reed, and G. Venkataramanan. Hierarchical control of bridge-of-bridge multilevel power converters. *Industrial Electronics, IEEE Transactions on*, 57(8):2679 – 2690, aug. 2010.
- [8] F. Kammerer, J. Kolb, and M Braun. A novel cascaded vector control scheme for the modular multilevel matrix converter. *IECON 2011 Melbourne*, Nov. 2011.